Joint Design of Trajectory and RF Pulses for Parallel Excitation

Chun-Yu Yip,[1]* William A. Grissom,[2] Jeffrey A. Fessler,[1,2] and Douglas C. Noll[2]

We propose an alternating optimization framework for the joint design of excitation k-space trajectory and RF pulses for small-tip-angle parallel excitation. Using Bloch simulations, we show that compared with conventional designs with predetermined trajectories, joint designs can often excite target patterns with improved accuracy and reduced total integrated pulse power, particularly at high reduction factors. These benefits come at a modest increase in computational time. Magn Reson Med 58:598–604, 2007. © 2007 Wiley-Liss, Inc.

Key words: joint design; parallel excitation; pulse design; trajectory design; alternating optimization

INTRODUCTION

With current excitation k-space (1) based methods of designing RF pulses for parallel excitation (2–5), one *predetermines* the gradient waveforms (hence, k-space trajectory), and subsequently designs the corresponding RF waveforms for a desired excitation pattern. In fact, trajectory predetermination may be unnecessarily restrictive, because the desired excitation pattern is known completely prior to design, unlike the analogous data acquisition process in which the object (and its spectrum) is unknown a priori. Perhaps, by *jointly* designing the trajectory and RF pulses, we might be able to exploit the design freedom to a fuller extent. The extra freedom could be channeled towards excitation accuracy improvement and/or pulse power reduction. Such benefits may be particularly significant in parallel excitation at high speedup factors, when the design problem becomes increasingly ill-posed, and "a proper interplay between the coil sensitivity profiles and the involved trajectories has to be found." (6)

There are surprisingly few studies on joint trajectory and pulse design in the literature. Hardy et al. (7) jointly optimized the gradient and RF waveforms for 2D single-coil selective excitation. They expressed both the gradient and RF waveforms as Fourier series, and applied simulated annealing to seek the Fourier coefficients that globally minimized the excitation error. For designing single-coil large-tip-angle pulses, Levin et al. (8) approximated the spiral trajectory by concentric circles and jointly optimized their radii together with the RF pulse.

In this note, we explore a new framework of joint trajectory and pulse design for parallel excitation. We propose that the joint design can be implemented as an alternating optimization process of trajectory parameters and RF pulses. In each iteration, the pulse optimization problem is solved using conjugate gradient (CG) (5), followed by a simple update of the trajectory parameters using gradient descent (GD). The cost function gradient, with respect to the trajectory parameters, can be computed efficiently using an analytical formula. This design process is efficient and produces trajectory and RF pulses that minimize the cost function *locally*. By Bloch equation simulation, we demonstrate that joint designs can excite target patterns with significantly improved accuracy and/or reduced total integrated pulse power, compared to designs with predetermined trajectories. These benefits come at a modest computational time cost, which is important because in most cases parallel excitation pulses have to be computed *online* (during scan session with subject inside scanner).

THEORY

Alternating Optimization

The joint design framework is an extension of the spatial-domain pulse design method (5) for parallel excitation. Consider pulse design for R-coil, small-tip-angle selective excitation in 2D, without loss of generality. Let $\mathbf{b}_r = (b_r(t_0), \ldots, b_r(t_{N-1}))$ be complex RF pulse samples for the rth coil, $r = 1, \ldots, R$, and $\mathbf{k}_x(\boldsymbol{\phi}_x) = (k_x(t_0; \boldsymbol{\phi}_x), \ldots, k_x(t_{N-1}; \boldsymbol{\phi}_x))$, $\mathbf{k}_y(\boldsymbol{\phi}_y) = (k_y(t_0; \boldsymbol{\phi}_y), \ldots, k_y(t_{N-1}; \boldsymbol{\phi}_y))$ be the excitation k-space trajectory parameterized by $\boldsymbol{\phi}_x = (\phi_{x_0}, \ldots, \phi_{x_{(L-1)}})$, $\boldsymbol{\phi}_y = (\phi_{y_0}, \ldots, \phi_{y_{(L-1)}})$, respectively. Let $\mathbf{A}(\mathbf{k}_x(\boldsymbol{\phi}_x), \mathbf{k}_y(\boldsymbol{\phi}_y))$ be the pulse design *system matrix* (5) as a function of the trajectory samples, and $\mathbf{S}_r = \mathsf{diag}(s_r(\mathbf{x}_0), \ldots, s_r(\mathbf{x}_{M-1}))$ be sensitivity pattern samples of the rth coil. The trajectory and RF pulses can be jointly designed via solving the following minimization problem:

$$(\hat{\boldsymbol{\phi}}_x, \hat{\boldsymbol{\phi}}_y, \hat{\mathbf{b}}_1, \ldots, \hat{\mathbf{b}}_R) = \underset{\boldsymbol{\phi}_x, \boldsymbol{\phi}_y, \mathbf{b}_1, \ldots, \mathbf{b}_R}{\arg\min} \Psi(\boldsymbol{\phi}_x, \boldsymbol{\phi}_y, \mathbf{b}_1, \ldots, \mathbf{b}_R) \quad [1]$$

where the cost function, Ψ, comprises total weighted squared excitation error and total integrated pulse power terms:

$$\Psi(\boldsymbol{\phi}_x, \boldsymbol{\phi}_y, \mathbf{b}_1, \ldots, \mathbf{b}_R) = \left\| \mathbf{d} - \sum_{r=1}^{R} \mathbf{S}_r \mathbf{A}(\mathbf{k}_x(\boldsymbol{\phi}_x), \mathbf{k}_y(\boldsymbol{\phi}_y)) \mathbf{b}_r \right\|_{\mathbf{W}}^2 + \beta \sum_{r=1}^{R} \|\mathbf{b}_r\|^2 \quad [2]$$

With Eq. [1], one seeks the trajectory parameters and RF pulses that produce an excitation pattern close to

[1]Department of Electrical Engineering and Computer Science, University of Michigan, Ann Arbor, Michigan.

[2]Department of Biomedical Engineering, University of Michigan, Ann Arbor, Michigan.

Grant sponsor: NIH; Grant number: DA15410

*Correspondence to: Chun-Yu Yip, Functional MRI Laboratory, University of Michigan, 2360 Bonisteel Ave., Ann Arbor, MI 48109-2108, USA. E-mail: chunyuy@umich.edu

Received 18 January 2006; revised 10 March 2007; accepted 15 March 2007.
DOI 10.1002/mrm.21262
Published online in Wiley InterScience (www.interscience.wiley.com).

the complex *desired excitation pattern*, $\mathbf{d} = (d(\mathbf{x}_0), \ldots, d(\mathbf{x}_{M-1}))$, with the secondary objective of reducing the total integrated power. These two objectives are balanced by regularization parameter β. Note that other regularization terms can be devised to control peak power (5) and trajectory smoothness. $\mathbf{W}$ is a diagonal matrix containing error weights for defining region of interest (ROI) (5).

Equation [1] can be implemented as the following *alternating* minimization process:

for $n = 0 : N_{alt} - 1$

$$\left(\hat{\boldsymbol{\phi}}_x^{(n+1)}, \hat{\boldsymbol{\phi}}_y^{(n+1)}\right) = \begin{cases} \left(\hat{\boldsymbol{\phi}}_x^{(0)}, \hat{\boldsymbol{\phi}}_y^{(0)}\right) & \text{if } n = 0, \\ \underset{\boldsymbol{\phi}_x, \boldsymbol{\phi}_y}{\arg\min}\, \Psi\left(\boldsymbol{\phi}_x, \boldsymbol{\phi}_y, \hat{\mathbf{b}}_1^{(n)}, \ldots, \hat{\mathbf{b}}_R^{(n)}\right) & \text{if } n \neq 0, \end{cases} \quad [3]$$

$$\left(\hat{\mathbf{b}}_1^{(n+1)}, \ldots, \hat{\mathbf{b}}_R^{(n+1)}\right) = \underset{\mathbf{b}_1, \ldots, \mathbf{b}_R}{\arg\min}\, \Psi\left(\hat{\boldsymbol{\phi}}_x^{(n+1)}, \hat{\boldsymbol{\phi}}_y^{(n+1)}, \mathbf{b}_1, \ldots, \mathbf{b}_R\right) \quad [4]$$

end

In words, by fixing the RF pulses from the nth iteration, we obtain the $(n+1)$th updated trajectory parameters via Eq. [3]; and subsequently by fixing the $(n+1)$th trajectory parameters, we design the $(n+1)$th optimal RF pulses via Eq. [4]. This alternating minimization process is initialized with $\left(\hat{\boldsymbol{\phi}}_x^{(0)}, \hat{\boldsymbol{\phi}}_y^{(0)}\right)$ and continues until $n = N_{alt} - 1$. The final trajectory and RF pulses, $\left(\mathbf{k}_x\left(\hat{\boldsymbol{\phi}}_x^{(N_{alt})}\right), \mathbf{k}_y\left(\hat{\boldsymbol{\phi}}_y^{(N_{alt})}\right)\right)$ and $\left(\hat{\mathbf{b}}_1^{(N_{alt})}, \ldots, \hat{\mathbf{b}}_R^{(N_{alt})}\right)$, are to be deployed on a parallel excitation system.

Both of the RF and trajectory optimization problems are constrained. The integrated and peak power constraints on the pulses can be handled via regularization (5). On the other hand, when computing $\left(\hat{\boldsymbol{\phi}}_x^{(n+1)}, \hat{\boldsymbol{\phi}}_y^{(n+1)}\right)$ via Eq. [3], we must ensure that the resulting trajectory satisfies the peak gradient amplitude and slew rate limits. Thus, Eq. [3] is constrained by

$$\begin{aligned} |D_1\mathbf{k}_x(\boldsymbol{\phi}_x)| \leqslant G_{\max}, \quad |D_2\mathbf{k}_x(\boldsymbol{\phi}_x)| \leqslant S_{\max}, \\ |D_1\mathbf{k}_y(\boldsymbol{\phi}_y)| \leqslant G_{\max}, \quad |D_2\mathbf{k}_y(\boldsymbol{\phi}_y)| \leqslant S_{\max}, \end{aligned} \quad [5]$$

where D_1 and D_2 are first and second order time-derivative operators, and $G_{\max}$, $S_{\max}$ are the peak gradient amplitude and slew rate, respectively. These constraints can be handled with special strategies of trajectory parameterization that will be discussed in the following section.

The pulse design problem (Eq. [4]) can be solved efficiently using CG (5); whereas the trajectory optimization (Eq. [3]) is a much more difficult nonlinear minimization problem, with many local minima in its cost function. It is possible to find its *global* minima using simulated annealing (7) or direct search methods such as Nelder–Mead (9). However, the computational cost of these algorithms is very high, rendering them unsuitable for the online joint design problem in which Eq. [3] has to be solved repetitively.

We instead solve Eq. [3] by applying the GD algorithm, and running it for a small number of iterations, possibly just one:

$$\begin{aligned} \hat{\boldsymbol{\phi}}_x^{(n+1)} &= \hat{\boldsymbol{\phi}}_x^{(n)} - \alpha\nabla_{\boldsymbol{\phi}_x}\Psi(\boldsymbol{\phi}_x, \boldsymbol{\phi}_y, \hat{\mathbf{b}}^{(n)})\Big|_{\left(\hat{\boldsymbol{\phi}}_x^{(n)}\hat{\boldsymbol{\phi}}_y^{(n)}\right)}, \\ \hat{\boldsymbol{\phi}}_y^{(n+1)} &= \hat{\boldsymbol{\phi}}_y^{(n)} - \alpha\nabla_{\boldsymbol{\phi}_y}\Psi(\boldsymbol{\phi}_x, \boldsymbol{\phi}_y, \hat{\mathbf{b}}^{(n)})\Big|_{\left(\hat{\boldsymbol{\phi}}_x^{(n)}\hat{\boldsymbol{\phi}}_y^{(n)}\right)}, \end{aligned} \quad [6]$$

where $\nabla_{\boldsymbol{\phi}_x}\Psi, \nabla_{\boldsymbol{\phi}_y}\Psi$ denote gradients of the cost function with respect to $\boldsymbol{\phi}_x, \boldsymbol{\phi}_y$, and α is a scaling factor on the update step. This CG-GD implementation of joint design leads to a set of *locally* optimal trajectory parameters and RF pulses, that potentially excites with higher accuracy and lower pulse power than a conventional design. Note that it is important to initialize the joint design with a good trajectory to avoid convergence to an undesirable local minima.

Trajectory Parameterization

We can reduce the dimension of the trajectory optimization problem via trajectory parameterization, provided that the number of parameters (L) is smaller than the number of trajectory samples (N). Also, using smooth basis functions may help enforcing the trajectory smoothness constraints (Eq. [5]). However, the obvious drawback is that our search is limited to a subspace of the original space of all implementable trajectories.

One parameterization strategy is to express k_x and/or k_y in terms of time-shifted basis functions, and regard the basis coefficients as parameters:

$$\begin{aligned} k_x(t_j; \boldsymbol{\phi}_x) &= \sum_{l=1}^{L} \phi_{xl} h_x(t_j - l\Delta t), \quad \text{and/or} \\ k_y(t_j; \boldsymbol{\phi}_y) &= \sum_{l=1}^{L} \phi_{yl} h_y(t_j - l\Delta t). \end{aligned} \quad [7]$$

Here, $h_x(t), h_y(t)$ are basis functions and Δt is a time shift. In matrix form,

$$\begin{aligned} \mathbf{k}_x(\boldsymbol{\phi}_x) &= \mathbf{H}_x\boldsymbol{\phi}_x, \quad \text{and/or} \\ \mathbf{k}_y(\boldsymbol{\phi}_y) &= \mathbf{H}_y\boldsymbol{\phi}_y, \end{aligned} \quad [8]$$

where $\mathbf{H}_x, \mathbf{H}_y$ are matrices whose columns are the time-shifted basis samples. By invoking the chain rule, we can easily relate the cost function gradients with respect to the parameters to that with respect to the trajectory samples:

$$\begin{aligned} \nabla_{\boldsymbol{\phi}_x}\Psi &= \mathbf{H}_x'\nabla_{\mathbf{k}_x}\Psi, \quad \text{and/or} \\ \nabla_{\boldsymbol{\phi}_y}\Psi &= \mathbf{H}_y'\nabla_{\mathbf{k}_y}\Psi. \end{aligned} \quad [9]$$

Because of the special form of system matrix $\mathbf{A}$, $\nabla_{\mathbf{k}_x}\Psi$ and $\nabla_{\mathbf{k}_y}\Psi$ can be computed analytically as follows:

$$\nabla_{\mathbf{k}_x}\Psi = 2Re\left\{\iota\sum_{r=1}^{R}\mathrm{diag}(\mathbf{b}_r')\mathbf{A}'\mathbf{X}\mathbf{S}_r'\mathbf{W}\mathbf{e}\right\}, \quad [10]$$

$$\nabla_{\mathbf{k}_y}\Psi = 2Re\left\{\iota\sum_{r=1}^{R}\mathrm{diag}(\mathbf{b}_r')\mathbf{A}'\mathbf{Y}\mathbf{S}_r'\mathbf{W}\mathbf{e}\right\}, \quad [11]$$

where $\iota = \sqrt{-1}$, excitation error $\mathbf{e} = \mathbf{d} - \sum_{r=1}^{R}\mathbf{S}_r\mathbf{A}(\mathbf{k}_x(\boldsymbol{\phi}_x), \mathbf{k}_y(\boldsymbol{\phi}_y))\mathbf{b}_r$, $\mathbf{X} = \mathrm{diag}(x_0, \ldots, x_{M-1})$ and $\mathbf{Y} = \mathrm{diag}(y_0, \ldots, y_{M-1})$. Derivation of these gradient expressions is included in the Appendix.

Example: Joint Design of Echo-Planar Pulses

Echo-planar (EP) RF pulses have been used widely in parallel excitation (3,4). Analogous to EP imaging, those pulses are designed with EP trajectories in excitation k-space that "frequency-encode" in one spatial dimension and "phase-encode" in the other. Accelerated EP trajectories under-sample the phase-encode dimension (k_y), and the resulting aliased excitation is resolved by the blurring effect of the Fourier transforms of the sensitivity patterns in k-space (because of the convolution process (2)), which leads to deposition of RF energy in between the phase-encoding lines.

An interesting question is whether nonuniform phase-encoding locations would be superior to uniform ones as used in (3,4), in terms of excitation accuracy and total integrated pulse power. In fact, it has been shown that non-uniform encoding in EP parallel imaging improves image quality (10). If non-uniform phase-encoding were indeed favorable in excitation, the optimal encoding locations would depend on the desired excitation pattern and sensitivity patterns specific to the experiment. The proposed joint design approach can be used to compute locally optimal phase-encoding locations and RF pulses.

Consider joint design with an EP trajectory, $\mathbf{k}(t_j) = (k_x(t_j), k_y(t_j))$, $j = 0 \ldots N-1$, for R-coil parallel excitation. One way to parameterize the trajectory is to approximate $k_y(t_j)$ as a sum of time-shifted rectangular (rect) functions, and leave $k_x(t_j)$ unparameterized. Let $\boldsymbol{\phi}_y = (\phi_{y_0}, \ldots, \phi_{y_{(L-1)}})$ be phase-encoding locations, T_{PE} be the duration of one phase-encoding line, and define rect function $h(t) = 1$ for $t \in [0, T_{\mathrm{PE}})$, and 0 otherwise. We can parameterize $k_y(t_j)$ by $\boldsymbol{\phi}_y$ via

$$k_y(t_j; \boldsymbol{\phi}_y) \approx \sum_{l=0}^{L-1}\phi_{yl}h(t_j - lT_{\mathrm{PE}}), \quad [12]$$

or in matrix-vector form, $\mathbf{k}_y(\boldsymbol{\phi}_y) \approx \mathbf{H}\boldsymbol{\phi}_y$, where $\mathbf{H}$ is a matrix whose columns are samples of the time-shifted rect functions. Provided that the y gradient blips underlying the phase-encoding are within the peak gradient and slew rate limits, this parameterization ensures that the constraints (Eq. [5]) are satisfied, resulting in a virtually constraint-free joint design. Now, one is ready to jointly design $\boldsymbol{\phi}_y$ and $\mathbf{b}_r, r = 1, \ldots, R$.

MATERIALS AND METHODS

We implemented the joint design of phase-encoding locations and EP pulses for a four-coil ($R = 4$) parallel excitation scenario, and compared it with a conventional design (5) using predetermined trajectory. EP trajectories with uniform phase-encoding were used to initialize the joint design, and as the predetermined trajectories for the conventional design. By 2D Bloch simulation (FOV = 24 cm × 24 cm, matrix size = 64 × 64), we investigated the benefits of optimizing phase-encoding locations in the joint design, in terms of excitation accuracy and total integrated power. All pulse designs and simulations were performed with Matlab R2006a (Mathworks, Natick, MA) on a 3.4 GHz Pentium workstation with 2 GB memory.

The uniform EP trajectories, used for joint design initialization and conventional design, under-sampled in the k_y dimension. They supported 1-cm excitation resolution in both x and y. We varied their phase-encode spacing, which was inversely proportional to y-direction excitation FOV (XFOV) ranging from 4 to 12 cm. It corresponded to a range of *speedup factors*, as defined in (5), from 6 down to 2. We compared the design methods at each speedup factor, anticipating that the joint design would be particularly beneficial in some particular range. All EP trajectories were produced by x, y gradient blips that complied with the peak gradient and slew rate constraints, which were 4 G/cm and 15,000 G/cm/s, respectively. Sampling period was 4 μs.

We compared the design methods for two desired excitation patterns. The first one was a 10 cm × 5 cm "horizontal block" of uniform 15-degree tip angle and zero phase, defined in a 24 cm × 24 cm FOV with matrix size of 64 × 64. The second pattern was a "vertical block" obtained by rotating the horizontal block by 90 degrees. Four out of eight of the complex receive sensitivity patterns (Fig. 1) of a

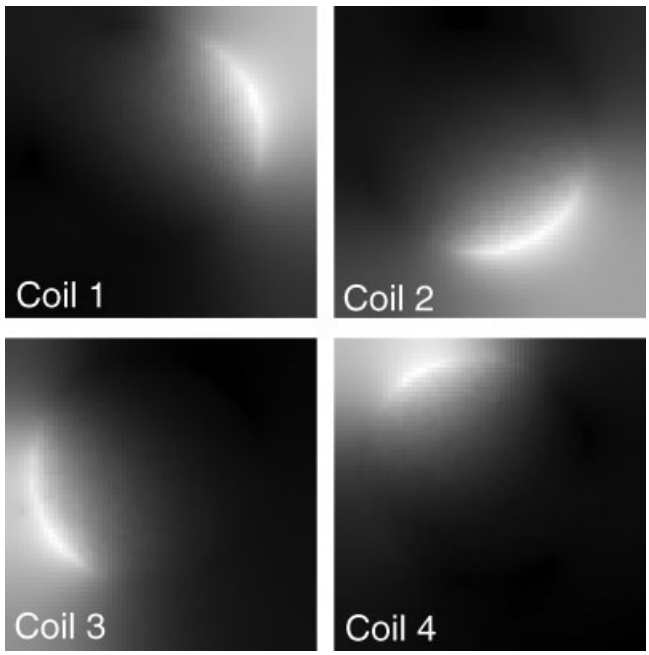

FIG. 1. Smoothed sensitivity patterns (magnitude, in a.u.) used in pulse designs and Bloch simulations.

head coil array (Intermagnetics, Latham, NY) were acquired as described in Ref. (5), and treated as transmit sensitivity patterns in both pulse designs and Bloch simulations. Relative weight of excitation error to pulse power in the cost function was matched for the conventional and joint designs ($\beta = 4000$). The ROI was derived via thresholding the body-coil phantom image (acquired for sensitivity map estimation). Off resonance effects were ignored in the pulse designs. In each alternation of the joint design, we ran 5 CG iterations for pulse design (Eq. [4]) and 1 GD trajectory parameter update (Eq. [3]), until convergence was reached (when current cost function value in CG was 99.9% of the previous one). We used the same convergence criterion for halting the conventional design. Each joint-design CG process was initialized by the pulse designed in the previous alternation (except in the first alternation, CG was initialized with a zero pulse). The scaling factor on the GD step was set small enough to ensure convergence ($\alpha = 5.2 \times 10^{-4}$).

RESULTS

Figure 2 compares the joint and conventional design methods, at different speedup factors, in terms of (a) normalized root-mean-square error (NRMSE) of the Bloch-simulated excitation pattern; (b) total integrated pulse power of all channels; (c) cost function (Eq. [2]) value when the methods reach convergence; and (d) computational time for the methods to reach convergence.

For the horizontal block desired excitation pattern (black solid lines), the joint design outperformed the conventional design in a range of high speedup factors—the

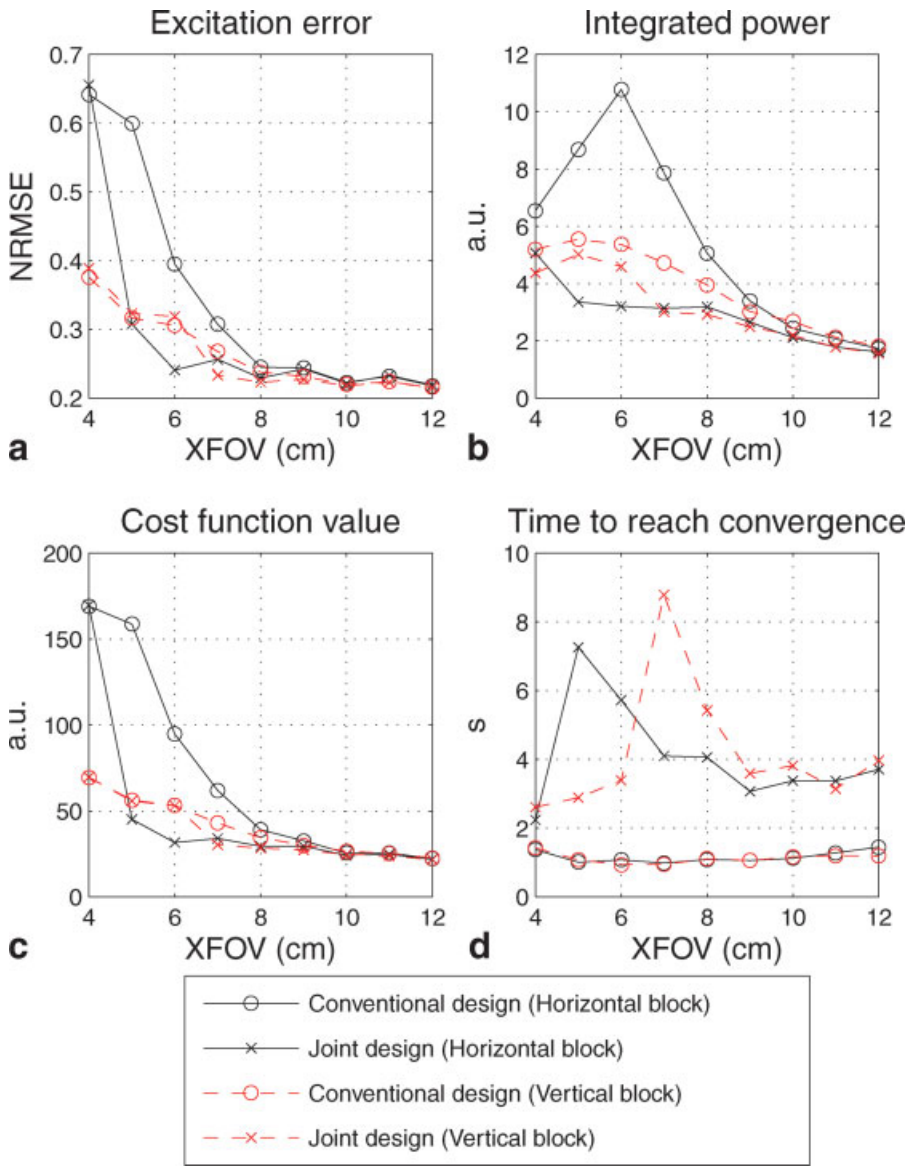

FIG. 2. Based on Bloch simulations, performance of the joint and conventional design methods are compared at different speedup factors. With cost in computational time, joint designs are often advantageous over the conventional designs, in terms of excitation accuracy and total integrated pulse power. This cost-benefit tradeoff is dependent on the choice of desired excitation pattern (in parentheses). [Color figure can be viewed in the online issue, which is available at www.interscience.wiley.com.]

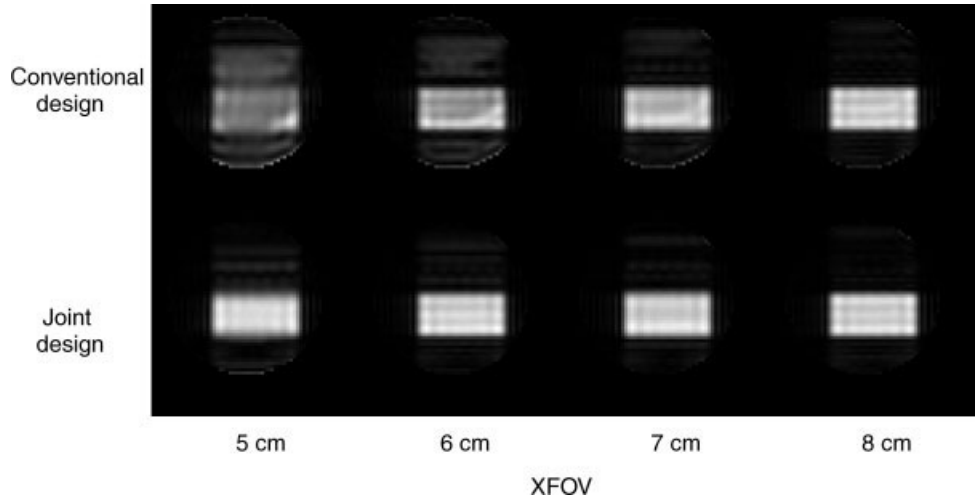

FIG. 3. Bloch-simulated excitation patterns (magnitude) by conventional and joint designs at high speedup factors. Adjustments of the phase encoding locations in the joint design lead to improved resolution of the aliased excitation.

jointly designed pulses achieved higher excitation accuracy and their total integrated power was lower (Fig. 2a,b). Figure 3 shows Bloch-simulated excitation patterns (magnitude) of the designs, at XFOV = 5–8 cm. The performance advantages diminished at low speedup factors. The superiority of the joint design at high speedup factors could be attributed to the lower cost function values that it attained (Fig. 2c), at the cost of increased computational time (Fig. 2d).

Figure 4a shows the uniform EP trajectory (at XFOV = 6 cm) used in the conventional method (and for initializing the joint design), and the non-uniform one that the joint design converged to. The joint design evidently adjusted the phase-encoding locations so that the central region of the desired excitation pattern spectrum (Fig. 4, underlying) became better sampled, leading to the observed excitation accuracy improvement and pulse power reduction.

We repeated the Bloch simulations for the vertical block desired excitation pattern (Fig. 2, red dashed lines), with identical design and simulation parameters. It was interesting that the previously observed margin in excitation accuracy at high speedup factors vanished, while a margin in total integrated power still existed, although it was smaller compared to the horizontal block case (Fig. 2a,b).

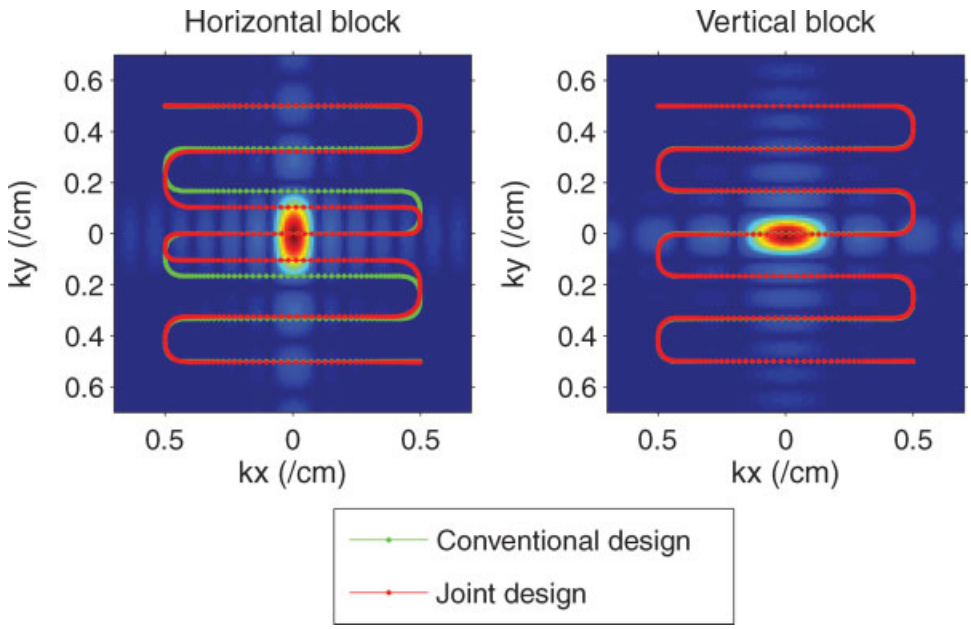

FIG. 4. EP trajectories with uniform phase-encoding used in the conventional method, and EP trajectories with encoding locations adjusted by the joint design method (XFOV = 6 cm). The adjustments, which are dependent on the specific desired excitation pattern, lead to improvement in excitation accuracy and reduction in total integrated pulse power. The improvement is particularly prominent at high reduction factors. (underlying: desired excitation pattern spectrum)

The cost function values that the methods attained were now close for all XFOVs, although the joint design still required significantly longer computational time to reach convergence (Fig. 2c,d). One can see, at XFOV = 6 cm for example, that the conventionally and jointly designed trajectories were almost identical (Fig. 4b). It suggested that the uniform phase encoding locations were in fact close to being locally optimal for this desired excitation pattern.

DISCUSSION

We have proposed a framework for the joint design of trajectory and RF pulses in parallel excitation. We illustrated that compared to conventional designs with predetermined trajectories, joint designs can often excite target patterns with significantly improved accuracy and/or reduced total integrated power. The improvements are particularly prominent at high reduction factors. The benefits come at modest expense of computational time, which could be affordable in practice. The cost-benefit tradeoff depends on the specific desired excitation pattern, and in fact, sensitivity patterns as well (results not shown).

Stability of the current joint design implementation (i.e., whether it converges to a local minimum or diverges) is sensitive to the threshold of cost function ratio in CG for declaring convergence (we used 99.9% in our simulations), and to a larger extent, the scaling factor on the GD step (α). To ensure convergence in EP pulse design, we experimented with the technique of *optimization transfer* (11) for updating the phase-encoding locations—we determined the step via constructing a quadratic *surrogate* function that lied above the original cost function, and minimizing it instead of the original cost. This approach guarantees a monotonic decrease in the cost function, effectively preventing divergence. However, applying optimization transfer to the pulse design problem requires a large amount of computation, which increases the total joint design computational time. Thus, it may not be favorable for online design purposes.

Besides EP trajectories, the joint design framework can be applied to various non-Cartesian trajectories. One can, for example, expand a spiral trajectory in basis functions such as splines, and jointly optimize the spline coefficient and RF pulses. However, the coefficients have to be updated without violating the peak gradient and slew rate constraints (Eq. [5]), rendering the trajectory update a constrained optimization problem. The joint design framework can also be applied to 3D excitation problems such as the design of 3D tailored RF pulses (12), although computational time might be too long to be practical.

APPENDIX

Deriving The Cost Function Gradients

The cost function (Eq. [2]) gradients, with respect to $\mathbf{k}_x$ and $\mathbf{k}_y$, provide the trajectory update direction in the GD step of the joint design. Because of the special form of system matrix $\mathbf{A}$ (5), the gradients can be derived algebraically. Let us define length-M error vector $\mathbf{e} = \mathbf{d} - \sum_{r=1}^{R} \mathbf{S}_r \mathbf{A}(\mathbf{k}_x(\boldsymbol{\phi}_x), \mathbf{k}_y(\boldsymbol{\phi}_y))\mathbf{b}_r$, and length-$N$ temporal vector

$$\begin{aligned}\mathbf{p}_x &= \nabla_{\mathbf{k}_x} \Psi \\ &= \nabla_{\mathbf{k}_x} \|\mathbf{e}\|_{\mathbf{W}}^2. \end{aligned} \quad [13]$$

The jth element of $\mathbf{p}_x$ is

$$p_{xj} = 2Re\{\mathbf{e}'\mathbf{W}\mathbf{q}_{xj}\}, \quad [14]$$

where $\mathbf{q}_{xj} = \frac{d}{dk_{xj}}\mathbf{e}$ is the derivative of $\mathbf{e}$ with respect to $k_x(t_j)$. The ith element of $\mathbf{q}_{xj}$ is given by

$$\begin{aligned} q_{xj,i} &= -\frac{d}{dk_{xj}} \left[\sum_{r=1}^{R} s_r(\mathbf{x}_i) \cdot \sum_{j=0}^{N-1} \exp(\imath k_{xj} x_i + \imath k_{yj} y_i) b_j \right] \\ &= -\sum_{r=1}^{R} s_r(\mathbf{x}_i) \cdot \imath x_i \cdot \exp(\imath k_{xj} x_i + \imath k_{yj} y_i) b_j. \end{aligned} \quad [15]$$

Thus,

$$\mathbf{q}_{xj} = -\sum_{r=1}^{R} \imath \mathbf{S}_r \mathbf{X} \mathbf{a}_j b_{jr}, \quad [16]$$

where $\mathbf{X} = \mathsf{diag}(x_0, \ldots, x_{M-1})$. Substituting Eq. [16] into Eq. [14] yields

$$\begin{aligned} p_{xj} &= 2Re\left\{ -\imath \mathbf{e}'\mathbf{W} \sum_{r=1}^{R} \mathbf{S}_r \mathbf{X} \mathbf{a}_j b_{jr} \right\} \\ &= 2Re\left\{ \imath \sum_{r=1}^{R} b'_{jr} \mathbf{a}'_j \mathbf{X} \mathbf{S}'_r \mathbf{W} \mathbf{e} \right\}. \end{aligned} \quad [17]$$

If we columnize $p_{xj}, j = 0, \ldots, N-1$, we obtain Eq. [10]:

$$\nabla_{\mathbf{k}_x} \Psi = 2Re\left\{ \imath \sum_{r=1}^{R} \mathsf{diag}(\mathbf{b}'_r) \mathbf{A}' \mathbf{X} \mathbf{S}'_r \mathbf{W} \mathbf{e} \right\}, \quad [18]$$

and defining $\mathbf{Y} = \mathsf{diag}(y_0, \ldots, y_{M-1})$ yields Eq. [11]:

$$\nabla_{\mathbf{k}_y} \Psi = 2Re\left\{ \imath \sum_{r=1}^{R} \mathsf{diag}(\mathbf{b}'_r) \mathbf{A}' \mathbf{Y} \mathbf{S}'_r \mathbf{W} \mathbf{e} \right\}. \quad [19]$$

REFERENCES

1. Pauly JM, Nishimura DG, Macovski A. A k-space analysis of small-tip-angle excitation. J Magn Reson 1989;81:43–56.
2. Katscher U, Börnert P, Leussler C, van den Brink JS. Transmit SENSE. Magn Reson Med 2003;49:144–150.
3. Zhu Y. Parallel excitation with an array of transmit coils. Magn Reson Med 2004;51:775–784.
4. Griswold MA, Kannengiesser S, Müller M, Jakob PM. Autocalibrated accelerated parallel excitation. In: Proceedings of the 13th Annual Meeting of ISMRM, Miami, 2005, number 2435.
5. Grissom WA, Yip C-Y, Zhang Z, Stenger VA, Fessler JA, Noll DC. A spatial domain method for the design of RF pulses in multi-coil parallel excitation. Magn Reson Med 2006;56:620–9.
6. Katscher U, Röhrs, J, Börnert P. Basic considerations on the impact of the coil array on the performace of Transmit SENSE. MAGMA 2005;18:81–88.

7. Hardy CJ, Bonomley PA, O'Donnnell M, Rocmer P. Optimization of two-dimensional spatially selective NMR pulses by simulated annealing. J Magn Reson 1988;77:233–250.
8. Levin YS, Pisani LJ, Spiclman DM, Pauly JM. Trajectory optimization for variable-density spiral two-dimensional excitation. In: Proceedings of the 14th Annual Meeting of ISMRM, Seattle 2006, number 3012.
9. Nelder JA, Mead R. A simplex method for function minimization. Comput J 1965;7:308–313.
10. Xu D, Ying L, Jacob M, Liang Z-P. Optimizing SENSE for dynamic imaging. In: Proceedings of the 13th Annual Meeting of ISMRM, Miami, 2005, number 2419.
11. Lange K, Hunter DR, Yang I. Optimization transfer using surrogate objective functions. J Comput Graph Stat 2000;9:1–20.
12. Yip C-Y, Fesster JA, Noll DC. Advanced three-dimensional tailored RF pulse for signal recovery in T_2^*-weighted functional MRI. Magn Reson Med 2006;56:1050–1059.